

RESEARCH ARTICLE SUMMARY

NEURODEVELOPMENT

Nests of dividing neuroblasts sustain interneuron production for the developing human brain

Mercedes F. Paredes^{*†}, Cristina Mora[†], Quetzal Flores-Ramirez[†], Arantxa Cebrian-Silla[†], Ashley Del Doso, Phil Larimer, Jiapei Chen, Gugene Kang, Susana Gonzalez Granero, Eric Garcia, Julia Chu, Ryan Delgado, Jennifer A. Cotter, Vivian Tang, Julien Spatazza, Kirsten Obernier, Jaime Ferrer Lozano, Maximo Vento, Julia Scott, Colin Studholme, Tomasz J. Nowakowski, Arnold R. Kriegstein, Michael C. Oldham, Andrea Hasenstaub, Jose Manuel Garcia-Verdugo, Arturo Alvarez-Buylla^{*}, Eric J. Huang^{*}

INTRODUCTION: Balance between excitatory and inhibitory neuron (interneuron) populations in the cortex promotes normal brain function. Interneurons are primarily generated in the medial, caudal, and lateral ganglionic eminences (MGE, CGE, and LGE) of the ventral embryonic forebrain; these subregions give rise to distinct interneuron subpopulations. In rodents, the MGE generates cortical interneurons, the parvalbumin⁺ (PV⁺) and somatostatin⁺ (SST⁺) subtypes that connect with excitatory neurons to regulate their activity. Defects in interneuron production have been implicated in neurodevelopmental and psychiatric disorders including autism, epilepsy, and schizophrenia.

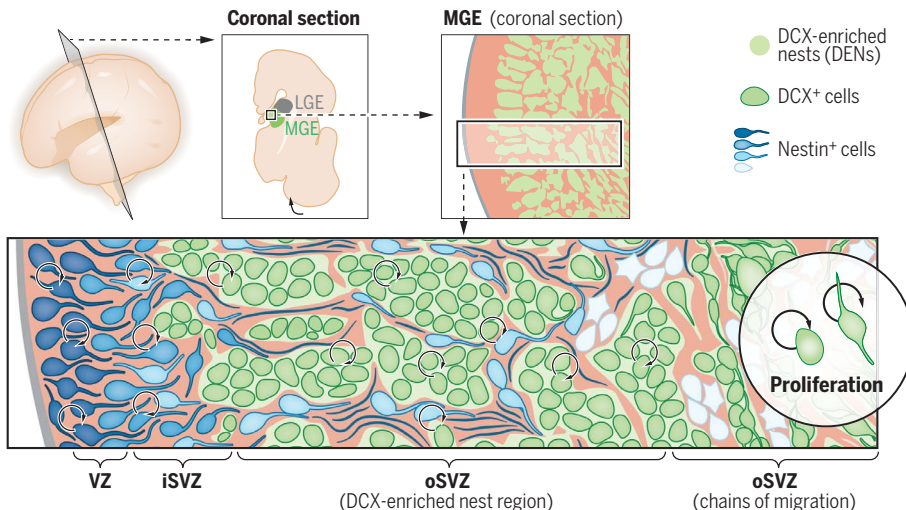
RATIONALE: How does the human MGE (hMGE) produce the number of interneurons required to populate the forebrain? The hMGE contains

progenitor clusters distinct from what has been observed in the rodent MGE and other germinal zones of the human brain. This cytoarchitecture could be the key to understanding interneuron neurogenesis. We investigated the cellular and molecular properties of different compartments within the developing hMGE, from 14 gestational weeks (GW) to 39 GW (term), to study their contribution to the production of inhibitory interneurons. We developed a xenotransplantation assay to follow the migration and maturation of the human interneurons derived from this germinal region.

RESULTS: Within the hMGE, densely packed aggregates (nests) of doublecortin⁺ (DCX⁺) and LHX6⁺ cells were surrounded by nestin⁺ progenitor cells and their processes. These DCX⁺ cell-enriched nests (DENs) were ob-

served in the hMGE but not in the adjacent LGE. We found that cells within DENs expressed molecular markers associated with young neurons, such as DCX, and polysialylated neural cell adhesion molecule (PSA-NCAM). A subpopulation also expressed Ki-67, a marker of proliferation; therefore, we refer to these cells as neuroblasts. A fraction of DCX⁺ cells inside DENs expressed SOX2 and E2F1, transcription factors associated with progenitor and proliferative properties. More than 20% of DCX⁺ cells in the hMGE were dividing, specifically within DENs. Proliferating neuroblasts in DENs persisted in the hMGE throughout prenatal human brain development. The division of DCX⁺ cells was confirmed by transmission electron microscopy and time-lapse microscopy. Electron microscopy revealed adhesion contacts between cells within DENs, providing multiple sites to anchor DEN cells together. Neuroblasts within DENs express PCDH19, and nestin⁺ progenitors surrounding DENs express PCDH10; these findings suggest a role for differential cell adhesion in DEN formation and maintenance. When transplanted into the neonatal mouse brain, dissociated hMGE cells reformed DENs containing proliferative DCX⁺ cells, similar to DENs observed in the prenatal human brain. This suggests that DENs are generated by cell-autonomous mechanisms. In addition to forming DENs, transplanted hMGE-derived neuroblasts generated young neurons that migrated extensively into cortical and subcortical regions in the host mouse brain. One year after transplantation, these neuroblasts had differentiated into distinct γ -aminobutyric acid-expressing (GABAergic) interneuron subtypes, including SST⁺ and PV⁺ cells, that showed morphological and functional maturation.

CONCLUSION: The hMGE harbors DENs, where cells expressing early neuronal markers continue to divide and produce GABAergic interneurons. This MGE-specific arrangement of neuroblasts in the human brain is present until birth, supporting expanded neurogenesis for inhibitory neurons. Given the robust neurogenic output from this region, knowledge of the mechanisms underlying cortical interneuron production in the hMGE will provide insights into the cell types and developmental periods that are most vulnerable to genetic or environmental insults. ■



Nests of DCX⁺ cells in the ventral prenatal brain. Schematic of a coronal view of the embryonic human forebrain showing the medial ganglionic eminence (MGE, green), with nests of DCX⁺ cells (DENs, green). Nestin⁺ progenitor cells (blue) are present within the VZ and iSVZ and are intercalated in the oSVZ (where DENs reside). The initial segment of the oSVZ contains palisades of nestin⁺ progenitors referred to as type I clusters (light blue cells) around DENs. In the outer part of the oSVZ, DENs transition to chains of migrating DCX⁺ cells; surrounding nestin⁺ progenitors are arranged into groups of cells referred to as type II clusters (white cells). In addition to proliferation of nestin⁺ progenitors, cell division is present among DCX⁺ cells within DENs, suggesting multiple progenitor states for the generation of MGE-derived interneurons in the human forebrain.

The list of author affiliations is available in the full article online.

*Corresponding author. Email: mercedes.paredes@ucsf.edu (M.F.P.); alvarezbuyllaa@ucsf.edu (A.A.-B.); eric.huang2@ucsf.edu (E.J.H.)

†These authors contributed equally to this work.

Cite this article as M. F. Paredes et al., *Science* **375**, eabk2346 (2022). DOI: 10.1126/science.abk2346

S READ THE FULL ARTICLE AT
<https://doi.org/10.1126/science.abk2346>

RESEARCH ARTICLE

NEURODEVELOPMENT

Nests of dividing neuroblasts sustain interneuron production for the developing human brain

Mercedes F. Paredes^{1,2,3,4*}, Cristina Mora^{5†}, Quetzal Flores-Ramirez^{1†}, Arantxa Cebrian-Silla^{2,6†}, Ashley Del Doso⁵, Phil Larimer¹, Jiapei Chen^{3,5}, Eugene Kang^{4,6}, Susana Gonzalez Granero⁷, Eric Garcia¹, Julia Chu¹, Ryan Delgado², Jennifer A. Cotter⁸, Vivian Tang⁵, Julien Spatazza⁶, Kirsten Obernier⁶, Jaime Ferrer Lozano⁹, Maximo Vento^{10,11}, Julia Scott¹², Colin Studholme^{13,14,15}, Tomasz J. Nowakowski^{2,16}, Arnold R. Kriegstein^{1,2,3,4}, Michael C. Oldham^{4,5,6}, Andrea Hasenstaub¹⁷, Jose Manuel Garcia-Verdugo⁷, Arturo Alvarez-Buylla^{2,3,4,6*}, Eric J. Huang^{2,3,4,5*}

The human cortex contains inhibitory interneurons derived from the medial ganglionic eminence (MGE), a germinal zone in the embryonic ventral forebrain. How this germinal zone generates sufficient interneurons for the human brain remains unclear. We found that the human MGE (hMGE) contains nests of proliferative neuroblasts with ultrastructural and transcriptomic features that distinguish them from other progenitors in the hMGE. When dissociated hMGE cells are transplanted into the neonatal mouse brain, they reform into nests containing proliferating neuroblasts that generate young neurons that migrate extensively into the mouse forebrain and mature into different subtypes of functional interneurons. Together, these results indicate that the nest organization and sustained proliferation of neuroblasts in the hMGE provide a mechanism for the extended production of interneurons for the human forebrain.

A proper balance between glutamatergic excitatory neurons and γ -aminobutyric acid (GABA)-expressing inhibitory neurons (GABAergic interneurons) is central to brain function. Deficits in GABAergic interneurons have been implicated in neurodevelopmental and psychiatric disorders

including autism, epilepsy, and schizophrenia (1–3). GABAergic cortical interneurons are primarily born in germinal zones of the embryonic ventral forebrain, including the medial and caudal ganglionic eminences (MGE and CGE) (4). Young interneurons born in the ganglionic eminences then undertake an extensive migration to reach the cortex and many other forebrain regions (5–7). After completing their migration, young neurons mature into different subtypes, including MGE-derived PV⁺ (parvalbumin-positive) and SST⁺ (somatostatin-positive) interneurons, that are required for normal cortical rhythms and cognitive function (8, 9). It remains unclear how the human MGE (hMGE) generates sufficient interneurons to meet the demand of the larger gyrencephalic cortex.

The hMGE can be delineated by the expression of transcription factor NKX2-1 (NK2 homeobox 1) (10, 11). An initial analysis of the hMGE described two types of nestin⁺ progenitor clusters around DCX⁺ (doublecortin-positive) and LHX6⁺ (LIM homeobox 6-positive) cells. Type I clusters contain nestin⁺ progenitor cell bodies and fibers located in the inner part of the outer subventricular zone (oSVZ), whereas type II progenitor clusters in the outer part of the oSVZ surround streams of DCX⁺/LHX6⁺ migrating young neurons (10). Here, we show that these aggregates of DCX⁺/LHX6⁺ cells in the hMGE, which we refer to as DCX⁺ cell-enriched nests (DENs), contain actively proliferating neuroblasts that persist until birth. Our data further suggest that hMGE cells can reform DENs in a xenograft

model and are a source of GABAergic neurons in the developing human brain.

Nests of DCX⁺ cells in the human MGE

We analyzed the hMGE between 14 and 39 gestational weeks (GW) (Fig. 1A and table S1). Using NKX2-1 staining to delineate the hMGE, we found that the size of hMGE increased between 14 and 22 GW (Fig. 1B). By 34 and 39 GW, the MGE became smaller but was still discernible as a wedge-shaped NKX2-1⁺ structure next to the ventricular wall (Fig. 1B). By cross-referencing NKX2-1 expression patterns and magnetic resonance imaging (MRI) of the human GE (12, 13), we found that the volume of the hMGE increased from 18 to 22 GW and decreased at 33 GW (Fig. 1, D and E). Next, we evaluated the expression of LHX6, a transcription factor activated by NKX2-1 that is necessary for subtype specification and migration of hMGE-derived interneurons (14, 15). Similar to NKX2-1, LHX6 expression was detected in the hMGE from 14 to 39 GW (fig. S1A). LHX6⁺ cells were organized into tight cellular aggregates, or nests (fig. S1, B and C). The majority of LHX6⁺ cells expressed DCX and PSA-NCAM (polysialylated neural cell adhesion molecule), another marker found in young migratory neurons (figs. S1C and S2C). Confocal imaging showed that radial glia fibers stained with nestin or vimentin encased DCX⁺ cells within the hMGE, a relationship that persisted from 14 to 39 GW (Fig. 1C and fig. S2, A and B). To better understand the configuration of these DCX⁺ nests (DENs), we performed serial coronal and axial (horizontal) mapping of the hMGE at 22 GW. Quantification of DEN size showed no change along the rostral-caudal (coronal) axis but a progressive increase in DEN size along the dorsal to ventral (axial) planes (Fig. 1, F and G). The average area of a DEN in coronal sections decreased by 53% between 14 and 39 GW (Fig. 1E).

A second germinal zone of the ventral telencephalon is the lateral ganglionic eminence (LGE) that sits immediately dorsal to the MGE. Work in rodents has shown that the LGE is a source of GABAergic projection neurons for the striatum and of interneurons for the olfactory bulb (16). In contrast to the hMGE, DCX⁺ cells in the hLGE were homogeneously distributed and showed no evidence of DEN formation (fig. S2B). The above results indicate that during a period of hMGE expansion and heightened neurogenesis, young DCX⁺/LHX6⁺ neurons become tightly packed into DENs surrounded by bundles of nestin⁺ and vimentin⁺ cells and fibers (type I clusters) in the first and early second trimester of hMGE development (10). DENs decreased in area with age, although they were still present at 39 GW. The persistent presence of DENs in

¹Department of Neurology, University of California, San Francisco, CA 94143, USA. ²Eli and Edythe Broad Institute for Stem Cell Research and Regeneration Medicine, University of California, San Francisco, CA 94143, USA.

³Biomedical Sciences Graduate Program, University of California, San Francisco, CA 94143, USA. ⁴Developmental and Stem Cell Graduate Program, University of California, San Francisco, CA 94143, USA. ⁵Department of Pathology, University of California, San Francisco, CA 94143, USA.

⁶Department of Neurological Surgery, University of California, San Francisco, CA 94143, USA. ⁷Laboratorio de Neurobiología Comparada, Instituto Cavanilles de Biodiversidad y Biología Evolutiva, Universitat de València–Centro de Investigación Biomédica en Red sobre Enfermedades Neurodegenerativas (CIBERNED), Valencia, Spain. ⁸Department of Pathology, Children's Hospital Los Angeles, and Keck School of Medicine of University of Southern California, Los Angeles, CA 90027, USA. ⁹Department of Pathology, Hospital Universitari i Politècnica La Fe, Valencia, Spain. ¹⁰Neonatal Research Group, Health Research Institute La Fe, Valencia, Spain. ¹¹Division of Neonatology, University and Polytechnic Hospital La Fe, Valencia, Spain. ¹²Department of Bioengineering, Santa Clara University, Santa Clara, CA 95053, USA. ¹³Biomedical Image Computing Group, Departments of Pediatrics, Bioengineering, and Radiology, University of Washington, Seattle, WA 98195, USA. ¹⁴Department of Bioengineering, University of Washington, Seattle, WA 98195, USA. ¹⁵Department of Radiology, University of Washington, Seattle, WA 98195, USA. ¹⁶Department of Anatomy and Department of Psychiatry and Behavioral Sciences, University of California, San Francisco, CA 94143, USA. ¹⁷Department of Otolaryngology, University of California, San Francisco, CA 94143, USA.

*Corresponding author. Email: mercedes.paredes@ucsf.edu (M.F.P.); alvarezbuyllaa@ucsf.edu (A.A.-B.); eric.huang2@ucsf.edu (E.J.H.). [†]These authors contributed equally to this work.

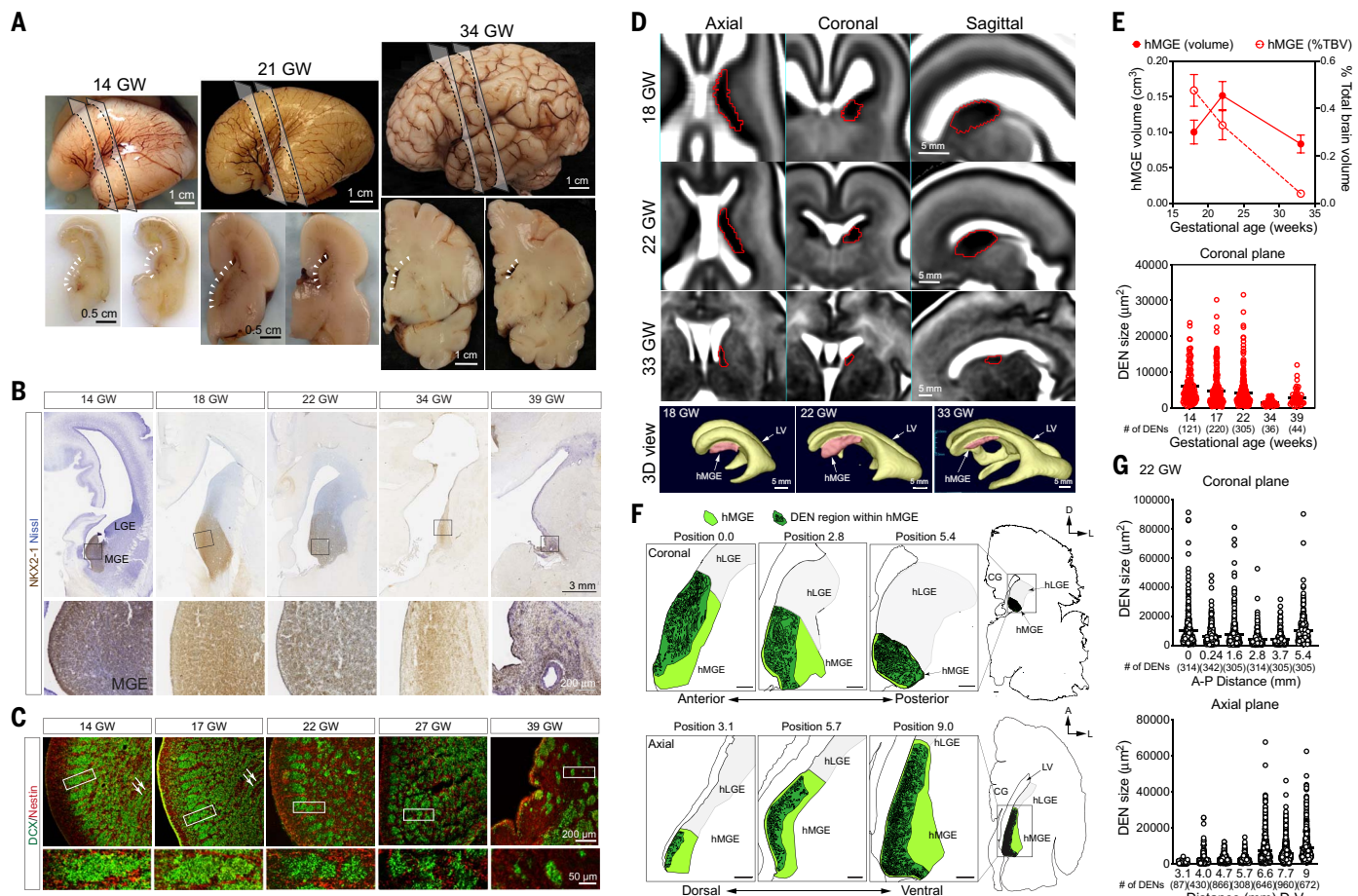


Fig. 1. hMGE organization in the prenatal and perinatal brain. (A) Lateral views (top) and coronal cross sections (bottom) of the prenatal human brain at 14, 21, and 33 GW. Dashed lines indicate the locations where the coronal sections are made; arrowheads indicate the location of human ganglionic eminences located next to the lateral walls of the lateral ventricles. (B) Immunohistochemical stains for NKX2-1 in the hMGE at 14, 18, 22, 34, and 39 GW. NKX2-1 shows a robust expression from 14 to 22 GW. Despite the decrease in hMGE size at 34 GW, NKX2-1 expression remains high. At 39 GW, NKX2-1 expression in the hMGE is reduced to a thin slit along the subventricular zone. (C) Confocal images of the hMGE from 14 to 39 GW reveal the unique organization of dense DCX⁺ nests that intermix with nestin⁺ fibers. (D) MRI images of prenatal hMGE (highlighted in red) on the axial, coronal, and sagittal planes at 18, 22, and 33 GW. Three-dimensional (3D) reconstruction highlights the position of the hMGE in relationship to the lateral ventricle (LV) at the respective ages. (E) Top: Quantification of hMGE volume relative to total brain volume by MRI images at 18, 22, and 33 GW. By cross-referencing NKX2-1 expression patterns and MRI images of human GE, we

found that hMGE volume increased from $115 \pm 15 \text{ mm}^3$ at 18 GW to $158 \pm 13 \text{ mm}^3$ at 22 GW, then decreased to $88 \pm 3 \text{ mm}^3$ at 33 GW. Data are means \pm SD; $n = 10$ for each gestational age. Bottom: Quantification of the size of DEN in hMGE on the coronal planes shows the progressive reduction in size from 14 to 39 GW. The average area of a DEN in coronal sections decreased from $6053 \pm 452 \mu\text{m}^2$ at 14 GW to $4052 \pm 242 \mu\text{m}^2$ at 22 GW, and dropped further to $2870 \pm 360 \mu\text{m}^2$ at 39 GW. The number of DENs for each gestational age is included in parentheses. (F) Schematic diagrams highlighting DENs (dark green) in hMGE (light green) in 22 GW prenatal brain at the coronal plane (top) and axial plane (bottom) reveal relatively similar sizes of DCX⁺ nests. The adjacent hLGE is shaded light gray. The positions of the hMGE indicated on the coronal plane are from anterior (position 0.0) to posterior (position 5.4). On the axial plane, the positions of the hMGE are from top (position 3.1) to bottom (position 9.0). Scale bars, 500 μm . (G) Top: Quantification of DEN size in the hMGE at 22 GW shows similar sizes from anterior to posterior on the coronal plane. Bottom: DEN size appears to become progressively larger from top to bottom on the axial plane.

the hMGE during an extended period of prenatal development suggests that this organization is fundamental to the production of inhibitory neurons in the human brain.

The majority of DCX⁺ cells within DENs appear destined to become GABAergic interneurons, as analysis at 14 and 39 GW showed that these cells expressed DLX2 (distal-less homeobox 2) (17, 18) (fig. S3A). In contrast to DLX2, ASCL1 (achaete-scute family BHLH transcription factor 1), frequently found in intermediate progenitors, was detected in

SOX2⁺ progenitors outside DENs (fig. S3B). Consistently, DEN cells also expressed GABA protein and glutamate decarboxylase (*GAD*) transcripts (fig. S3, C and D). These results further suggest that DCX⁺ cells within DENs are early GABAergic interneurons.

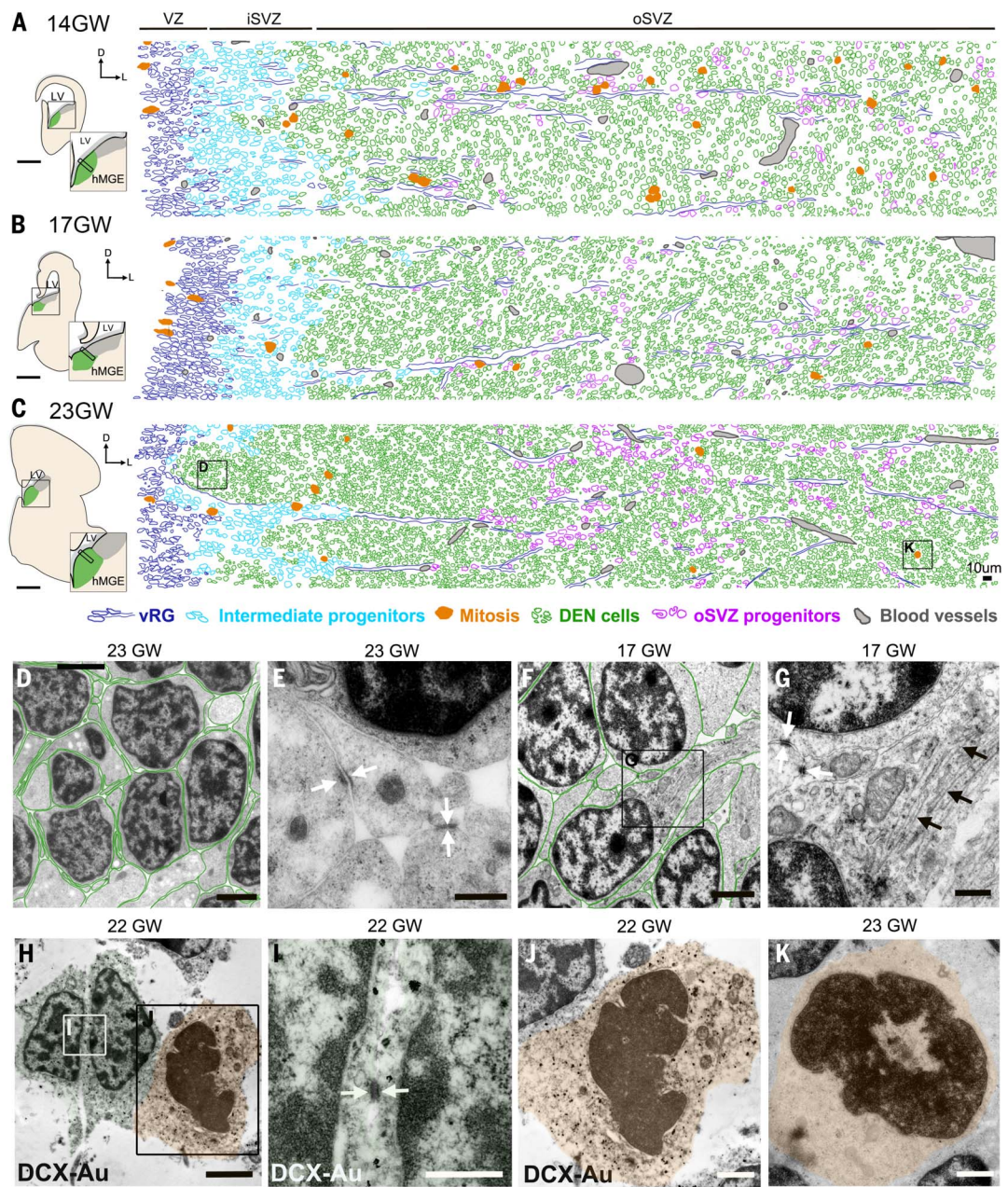
Ultrastructural and transcriptomic features define DENs

We next used transmission electron microscopy (TEM) to analyze the hMGE at 14, 17, and 23 GW. DENs were identified as nests of cells

separated by bundles of radial glia fibers (Fig. 2, A and C). Cells within the DENs had a small nucleus with dark nucleoplasm, heterochromatin clumps, scarce cytoplasm with many free ribosomes, and frequent small adherens junctions (<200 nm in length) (Fig. 2, D to G), features seen in young neurons (19, 20). Immunogold TEM staining confirmed that cells in DENs were DCX⁺ (Fig. 2, H and I). In addition to the DEN cells, we identified ventricle-contacting radial glia (vRG) and other progenitor cells in the iSVZ and oSVZ

Fig. 2. Ultrastructural characteristics of DENs in the hMGE.

(A to C) Schematics of 14, 17, and 23 GW hMGE in coronal sections used to map identified cell types in TEM ultrathin section micrographs. Ventricular radial glia (vRG) (dark blue), intermediate progenitors (cyan), mitoses (orange), DEN cells (green), outer subventricular zone (oSVZ) progenitors (purple), and blood vessels (gray) were identified by ultrastructural characteristics (table S2 and fig. S4). (D) DEN cells close to the lateral ventricle in (C) showed scarce cytoplasm and thin interdigitated expansions oriented in all directions (DEN cell cytoplasm outlined in green). (E) High magnification of DEN cell expansions showing frequent small adherens junctions (white arrows). (F and G) DEN cells deep into the hMGE showing long cell expansions rich in mitochondria and microtubules (black arrows). Note that contacts through small adherens junctions were frequent (white arrows). (H to J) Immunogold TEM of DCX⁺ cells within DENs in 22 GW hMGE. Note that DCX-Au⁺ cells show scarce cytoplasm and small adherens junctions (white arrows). DCX-Au⁺ mitotic figures inside DENs were also observed. (K) Mitotic figure within DEN in (C). Scale bars, 0.5 mm [(A) to (C)], 2 μm [(D), (F), and (H)], 500 nm [(E), (G), and (I)], 1 μm [(J) and (K)].



Downloaded from https://www.science.org at University Van Amsterdam on April 13, 2025

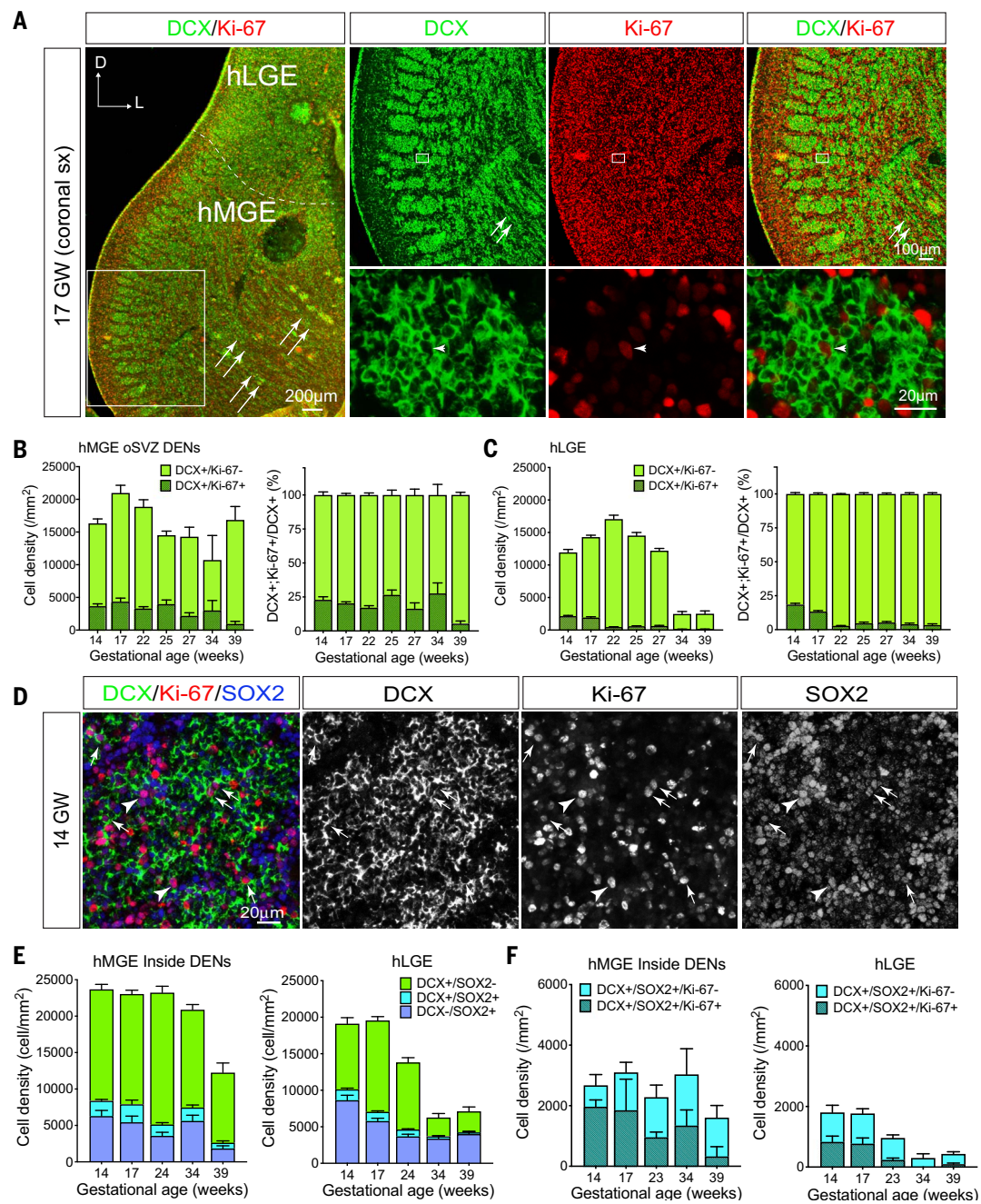
(table S2). vRG contacted the ventricle through thin apical expansions that had apical junctions and a primary cilium. Their nuclei were elongated and irregular and frequently had nuclear envelope chromatin sheets (21, 22) (fig. S4, A to D). In the iSVZ, progenitor cells had more rounded nuclei than vRG and a higher number of heterochromatin clumps. iSVZ progenitors lacked apical junctions, indicating that they were not part of the ventricular epithelium (fig. S4, E and F). Prominent bundles of stacked radial glia expansions rich in intermediate filaments and microtubules were noted in oSVZ at all ages studied (Fig. 2, A to C, and fig. S4, L to O). These bundles correspond to type I clusters of radial glia fibers previously described

(10) and contain an interspersed third type of progenitor cell with fewer intermediate filaments and a morphology that resembles outer-radial glia-like cells (fig. S4, H to K). MGE cells, including cells within DENs, at all ages studied had a cytoplasmic cylindrical structure that we refer to as ribosomal barrels, containing membrane lamellae with ribosomes lining the inner side (fig. S4, P and Q). The function of ribosomal barrels, or lamellae, is unknown.

On the basis of this cell classification scheme, we used tiled high-resolution TEM images to reconstruct the cellular composition of the hMGE at 14, 17, and 23 GW (Fig. 2, A to C). These reconstructions revealed the location of DENs and their consolidation with age.

Mitoses were frequent in the VZ and iSVZ, and within and around DENs, at the three gestational ages studied (Fig. 2, A to C, and fig. S4, R to T). At 14 GW, we noted that the majority of mitoses were associated with radial glia bundles, but by 17 and 23 GW, mitotic figures were among DEN cells (Fig. 2 and fig. S4, fuchsia). Using immunogold staining at 22 GW, we confirmed that mitoses within DENs were DCX⁺ (Fig. 2, H to J). These results suggested that a subpopulation of DEN cells were proliferative between 14 and 23 GW (Fig. 2, J and K). By 23 GW, cells in DENs closer to the VZ had thin interdigitated expansions oriented in all directions (Fig. 2, D and E). In contrast, DEN cells located farther away from the ventricle (~900 μm) had more polyribosomes

Fig. 3. DCX⁺ cells proliferate in the human ganglionic eminences. (A) Left: Confocal image of a coronal section of 17 GW hMGE and hLGE immunostained with DCX (green) and Ki-67 (red). Dashed line highlights the boundary that separates the hLGE and hMGE; arrows indicate streams of DCX⁺ cells migrating away from DENs at the edge of the hMGE. Right: Higher magnifications of DENs in the boxed area in the left panel (top row) where many DCX⁺ cells show positive staining for Ki-67 (bottom row); arrowhead points to a DCX⁺/Ki-67⁺ cell in the DENs. (B and C) Quantification of DCX⁺/Ki-67⁺ cells and DCX⁺/Ki-67⁻ cells in hMGE (B) and hLGE (C) at 14, 17, 22, 25, 27, 34, and 39 GW. DCX⁺/Ki-67⁺ cells and DCX⁺/Ki-67⁻ cells are presented as cell density (number of cells per mm²) (left panels); in addition, DCX⁺/Ki-67⁺ cells are presented as the percentage of DCX⁺ cells (right panels). Data are means \pm SEM. (D) Confocal images of hMGE at 14 GW immunostained with DCX, Ki-67, and SOX2 antibodies. Arrows in the merged panel and individual channels highlight DCX⁺/SOX2⁺/Ki-67⁺ cells; arrowhead indicates a DCX⁺/SOX2⁺/Ki-67⁺ cell within DENs. (E and F) Quantifications of DCX⁺/SOX2⁻, DCX⁺/SOX2⁺, and DCX⁺/SOX2⁺ progenitors (E) and DCX⁺/SOX2⁺ progenitors that are still in the cell cycle (Ki-67⁺) or already exited cell cycle (Ki-67⁻) (F) in hMGE and hLGE at 14, 17, 24, 34, and 39 GW. Data are means \pm SEM and are presented as cell density (number of cells per mm²).



and mitochondria, and their expansions were thicker and longer; this may reflect a higher degree of differentiation and activation of the migratory stage away from the MGE (Fig. 2, F and G, and table S2).

The organization of progenitor cells in the hMGE, which differs from that of neighboring hLGE, suggests that the pattern of gene expression responsible for DEN formation may be specific to the MGE. Using public microdissected hLGE and hMGE transcriptomic data (23), we performed gene coexpression analysis (24) from 17, 18, 23, and 23.5 GW samples (fig. S5A). This analysis revealed a group of genes highly correlated in their

expression in the hMGE at all ages studied (the sienna3 module; fig. S5B). This module included genes implicated in neuronal stem cell population maintenance, regulation of cell-substrate adhesion, homophilic cell adhesion, and extracellular matrix organization. The expression of all these genes decreased with gestational age. Among the top genes in the sienna3 module, there were several cell adhesion-related nonclustered protocadherin genes (*PCDH17*, *PCDH10*). Immunostaining at 22 GW showed that *PCDH10*⁺ cells were located almost exclusively outside DENs. In the 22 GW hLGE, *PCDH10*⁺ was widely distributed, interspersed between DCX⁺ cells (fig. S5C).

Another protocadherin gene found in this module, *PCDH19*, showed robust and extensive expression in the 22 GW hMGE that colocalized with DCX⁺ cells within DENs (fig. S5D); *PCDH19*⁺ cells were not detected in the hLGE (fig. S5D).

In addition to the sienna3 module, a second module (greenyellow) enriched in the hMGE contained genes implicated in regulating the cell cycle, DNA replication, and mitotic nuclear division (fig. S5E). The gene expression differences within this module between the hMGE and hLGE increased with age. Immunostains showed that E2F1 (E2F transcription factor 1), a top gene in this module, was

enriched as punctate staining in the 22 GW hMGE, but not in hLGE. E2F1 staining frequently overlapped with DCX staining. Unlike DCX⁺ cells in the hMGE that frequently expressed E2F1, DCX⁺ cells in hLGE were E2F1⁻ (fig. S5F). Together with the presence of mitosis in DCX⁺ cells (Fig. 2, H to J), these results suggest that a subpopulation of DCX⁺ neuroblasts in DENs have proliferative capacity.

Proliferating DCX⁺ cells within DENs

To further characterize the proliferation of cells within DENs, we performed immunostains for Ki-67, a protein expressed in dividing cells. Proliferating neuroblasts (DCX⁺/Ki-67⁺ cells) were detected in both the hMGE and hLGE from 14 to 39 GW (Fig. 3A). In the hMGE, DCX⁺ cells were primarily located within DENs (Fig. 3B and fig. S6B) and a substantial fraction of all dividing (Ki-67⁺) cells in the hMGE were DCX⁺ (31% at 14 GW, 21% at 17 GW, and 24% at 23 GW). The proportion of DCX⁺ cells in DENs that were Ki-67⁺ remained at 20 to 25% from 14 to 34 GW and dropped to ~5% at 39 GW (Fig. 3B). Ki-67⁺ cells were observed both in the center and close to the edge of DENs. Similarly, ~20% of the DCX⁺ cells in the hLGE were Ki-67⁺ at 14 and 17 GW, but these proportions in the LGE decreased to ~3% between 17 and 22 GW; by 22 GW, DCX⁺/Ki-67⁺ cells were rare in the hLGE (Fig. 3C).

Using SOX2 as a marker for undifferentiated progenitor cells (25, 26), we found that the majority of SOX2⁺ cells were located outside DENs (fig. S6, A and C), consistent with previous observations (10). However, a subpopulation of DCX⁺ cells in DENs also expressed SOX2, and more than 50% of these DCX⁺/SOX2⁺ cells were Ki-67⁺ (Fig. 3D, arrows). DCX⁺/SOX2⁺/Ki-67⁺ or DCX⁺/SOX2⁺/Ki-67⁺ cells could still be detected in the hMGE at 39 GW (Fig. 3, E and F, and fig. S6B), but these cells were rarely observed outside DENs from 14 to 34 GW (fig. S6A). The hLGE contained fewer DCX⁺/SOX2⁺ cells than the hMGE. Consistent with the above data, DCX⁺/SOX2⁺ cells in the hLGE could be observed at 14 and 17 GW (Fig. 3, E and F), but their numbers dropped between 17 and 23 GW and there were very few at 34 and 39 GW (Fig. 3, E and F). Like the DCX⁺/SOX2⁺ cells, a number of SOX2⁺ progenitors were Ki-67⁺ in both the hMGE and hLGE. The number of SOX2⁺/Ki-67⁺ progenitors decreased earlier in the hLGE (by 23 GW) than in the hMGE (34 GW) (fig. S6C). To validate the proliferative properties of DCX⁺ cells, we infected 18 GW hMGE slice cultures with CMV-GFP adenovirus (adenovirus expressing green fluorescent protein under a CMV promoter) to label cells and used time-lapse confocal imaging to follow proliferative behavior during 72 hours (fig. S7A). Dividing cells displaying interkinetic migration in the VZ (movie S1), but more than half (56%) of the

observed mitoses ($n = 122$) occurred deeper in the hMGE in the iSVZ and oSVZ. Among these divisions, we noted cells that showed mitotic somatic translocation typical of outer radial glia progenitor cells (27). We also observed cells with processes after division that corresponded to DCX⁺ cells in post hoc immunostaining (fig. S7, B and C, and movie S2). Quantification of the cellular populations in the slices showed that 27% of DCX⁺ cells in hMGE cultures expressed Ki-67, similar to what was observed in the postmortem quantifications (Fig. 3B). Taken together, our results indicate that a subpopulation of DCX⁺ neuroblasts in the hMGE continues to proliferate within DENs.

Transplanted hMGE cells recapitulate DEN features

We next investigated whether hMGE development could be recapitulated by xenotransplantation (7, 28). We dissected the hMGE from 14 to 16 GW samples and transplanted the dissociated hMGE cells into the cortex of immunosuppressed recipient animals. Transplanted cells, identified by the expression of human nuclear antigen (HNA), were analyzed at 45, 90, and 365 days after transplant (DAT). At 45 and 90 DAT (corresponding to hMGE cells at ~21 GW and 26 GW, respectively), transplanted cells formed large masses of densely packed HNA⁺ cells around the injection site (Fig. 4B); HNA⁺ cells expressed NKX2-1 at 45 DAT (86%) and 90 DAT (94%) (Fig. 4C and fig. S8D), but not SP8 or COUP transcription factor 2 (COUPTFII), associated with LGE and CGE, respectively (fig. S8, A to C). These results supported the ability of the transplanted hMGE cells to maintain their regional identity. At 45 DAT, HNA⁺ cells became organized into nests of DCX⁺ cells encased by vimentin⁺ radial glial fibers and cells, similar to the DEN architecture found in the intact hMGE in vivo (Fig. 4D). HNA⁺/DCX⁺ DENs were also identified at 90 DAT, but these were smaller and had fewer cells (Fig. 4E and fig. S9A).

The ability of the transplanted hMGE progenitors to organize as DENs (Fig. 4D and fig. S9A) raised the possibility that the transplant-derived DCX⁺ nests retain proliferative activity as observed in vivo. We quantified the proportion of all HNA⁺ transplant-derived cells that were Ki-67⁺. Within the transplant mass, we found that 23% of all HNA⁺ cells were Ki-67⁺ at 45 DAT, dropping to 3.5% by 90 DAT (fig. S10, A to C). By 365 DAT, no HNA⁺/Ki-67⁺ cells were present (fig. S10B). Of all HNA⁺/DCX⁺ cells in the transplant mass at 45 DAT, 19% were Ki-67⁺, similar to the 20 to 25% of DCX⁺ cells that were in the cell cycle in the post mortem DENs at 17 to 22 GW (fig. S10D). Among the Ki-67⁺/HNA⁺ cells, about half (58%) were DCX⁺ at 45 DAT. However, HNA⁺/DCX⁺ cells that

migrated outside the transplant were Ki-67⁺, which suggests that as hMGE-derived young neurons become migratory, they stop dividing.

To further characterize the cellular composition close to the transplant site, we performed immunostains for DCX and SOX2. At 45 DAT, ~35% of HNA⁺ cells were DCX⁺/SOX2⁺, ~45% were DCX⁺/SOX2⁻, and ~20% were DCX⁻/SOX2⁺ ($n = 4$) (Fig. 4, E and F). By 90 DAT, the majority of SOX2⁺ cells were no longer DCX⁺ ($n = 2$). DCX⁺/SOX2⁺ cells made up 36.6% of the HNA⁺/Ki-67⁺ population at 45 DAT and 13.2% at 90 DAT (Fig. 4, G and H). As observed in vivo, a fraction of the Ki-67⁺ cells within the transplant mass were DCX⁺/SOX2⁻ (~10%) at 45 and 90 DAT. By 365 DAT, most of the transplant mass disappeared, and the remaining HNA⁺ cells did not express DCX or Ki-67 (Fig. 4H). Taken together, these results indicate that hMGE progenitor cells transplanted into the mouse brain grew into a mass of cells that mimicked the composition and self-organization of the hMGE, including the formation of DENs.

Transplanted hMGE cells display properties of interneurons

We noted that at 45 DAT, HNA⁺/DCX⁺ cells were dispersing away from DENs and the transplant site (Fig. 5A); the majority of these cells had a migratory morphology. More than 99% of the dispersing hMGE cells at 45 and 90 DAT were DCX⁺ (99.1% and 99.4%, respectively), but at both these ages, the majority of HNA⁺/DCX⁺ cells were NKX2-1⁻, consistent with the down-regulation of this transcription factor in migrating GABAergic interneurons (29). HNA⁺/DCX⁺ cells were observed as far as 3 mm from the transplant site at 45 and 90 DAT, respectively (fig. S9B). From these results, we infer that hMGE-derived transplanted cells are migratory in the brain of juvenile mice. To study this migratory behavior, we infected 14 GW hMGE-dissociated cells with lentiviruses that expressed GFP under the control of *DLX1/2* (distal-less homeobox 1/2) enhancer (*i12b*-GFP lentivirus) and transplanted these cells into the neonatal mouse cortex. GFP⁺ hMGE cells were recorded at 21 DAT in organotypic slices prepared for time-lapse microscopy (Fig. 5C). Individual GFP⁺ cells had a migratory behavior similar to that observed in mouse cortical interneurons (30), including extension of a leading process (frequently bifurcated) and nucleokinesis. Cells outside the transplant moved at an average speed of 21 $\mu\text{m}/\text{hour}$ (Fig. 5C). We also noted movements of cells within the transplant (movie S3), but the high cell density prevented us from precisely following the movement of individual cells and determining their migratory behavior.

By 90 DAT, HNA⁺ cells were observed leaving the injection site as DCX⁺ chains (Fig. 5, D and E), and individual DCX⁺ cells

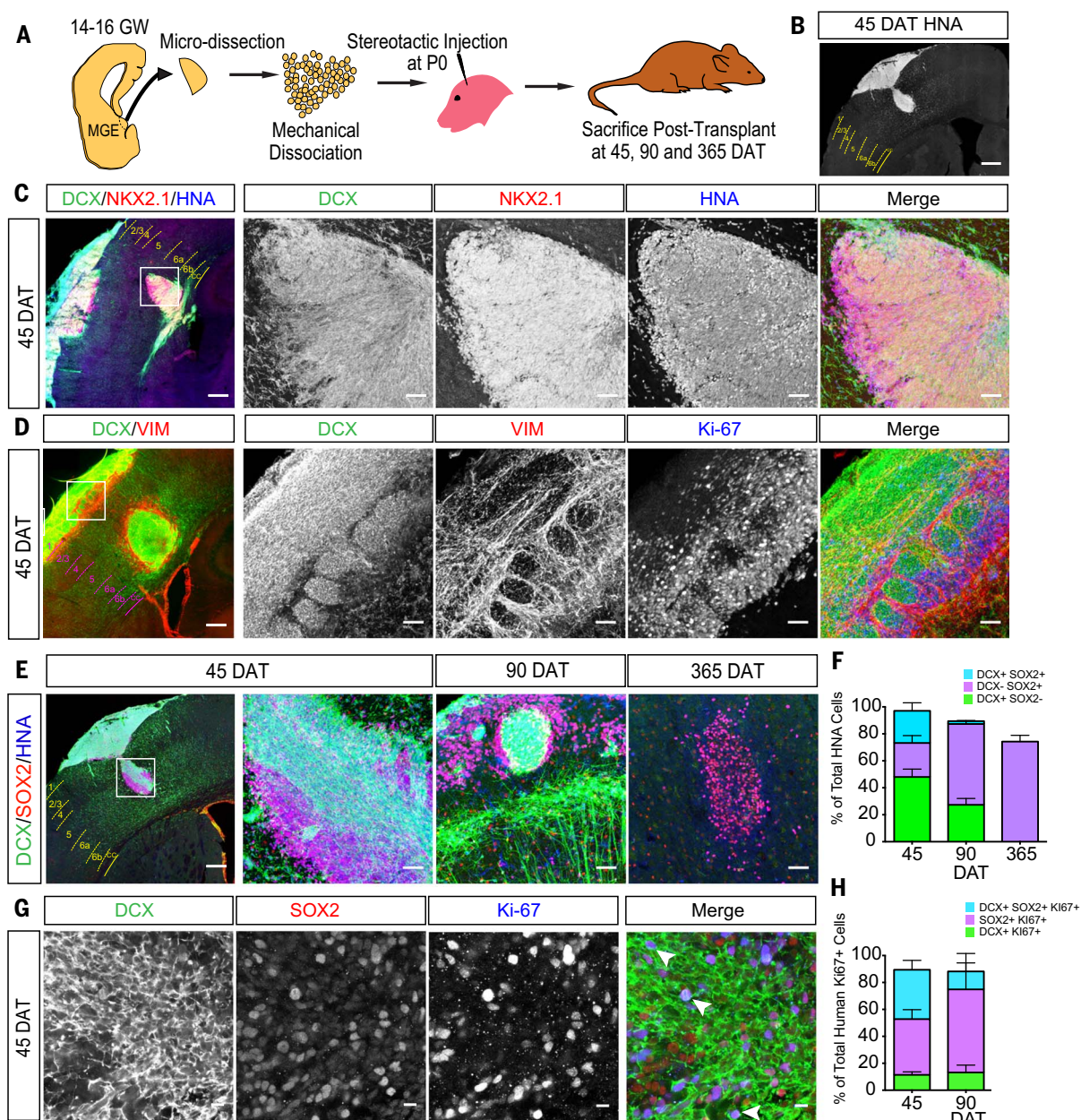


Fig. 4. Transplanted hMGE cells recapitulate DEN organization and proliferation. (A) Schematic of hMGE transplantation surgery. (B) Coronal section indicating injection site of HNA⁺ cells (white) at 45 DAT. Dashed lines delimit cortical layers; cc, corpus callosum. (C) HNA⁺ cells at the injection site at 45 DAT express DCX and NKX2.1. The transplant (boxed area of the leftmost panel) is shown at higher magnification. (D) Transplanted hMGE cells form dense DCX⁺ nests encased by VIM⁺ radial glia fibers at the site of injection at 45 DAT. The transplant (boxed area of the leftmost panel) is shown at higher magnification. Many VIM⁺ and DCX⁺ cells are Ki-67⁺. (E) HNA⁺ (blue) cells at injection sites

express DCX and SOX2 at 45, 90, and 365 DAT. (F) Quantification of proportion of total HNA⁺ cells at the injection site (45 DAT, $n = 4$; 90 DAT, $n = 2$; 365 DAT, $n = 3$) that are DCX⁺ (green), SOX2⁺ (purple), or DCX⁺/SOX2⁺ (cyan). Data are means \pm SEM. (G) High magnification of DCX⁺, SOX2⁺, and Ki-67⁺ cells in DENs at 45 DAT. (H) Quantification of proportion of HNA⁺/Ki-67⁺ cells at the injection site (45 DAT, $n = 4$; 90 DAT, $n = 2$; 365 DAT, $n = 3$) that are DCX⁺ (green), SOX2⁺ (purple), or DCX⁺/SOX2⁺ (cyan). Data are means \pm SEM. Scale bars, 500 mm [(B) and leftmost panel in (C) to (E)], 50 μ m [other panels in (C) to (E)], 10 μ m (G).

were found dispersed into many regions of the mouse brain including the hippocampus, amygdala, corpus callosum, striatum, septum, olfactory bulb, and piriform cortex (fig. S11). Relative to 45 DAT, most of the hMGE-derived cells at 90 DAT exhibited a more complex neuronal morphology with

increased branch number and length (Fig. 5, A and B, and fig. S11). At 90 DAT, a subpopulation of the DCX⁺/HNA⁺ cells expressed GABA (Fig. 5E), but these cells were negative for the mature neuronal marker NeuN. By 210 DAT, the expression of DCX was reduced (fig. S12, A and B); a fraction of hMGE-derived cells

were NeuN⁺ and several expressed the interneuron subtype marker SST (fig. S12C), which suggested that these cells had begun their differentiation (fig. S12C). By 365 DAT, most HNA⁺/NeuN⁺ cells expressed GABA, with many expressing SST and some rare cells expressing PV⁺, calbindin⁺, or calretinin⁺ (Fig. 5,

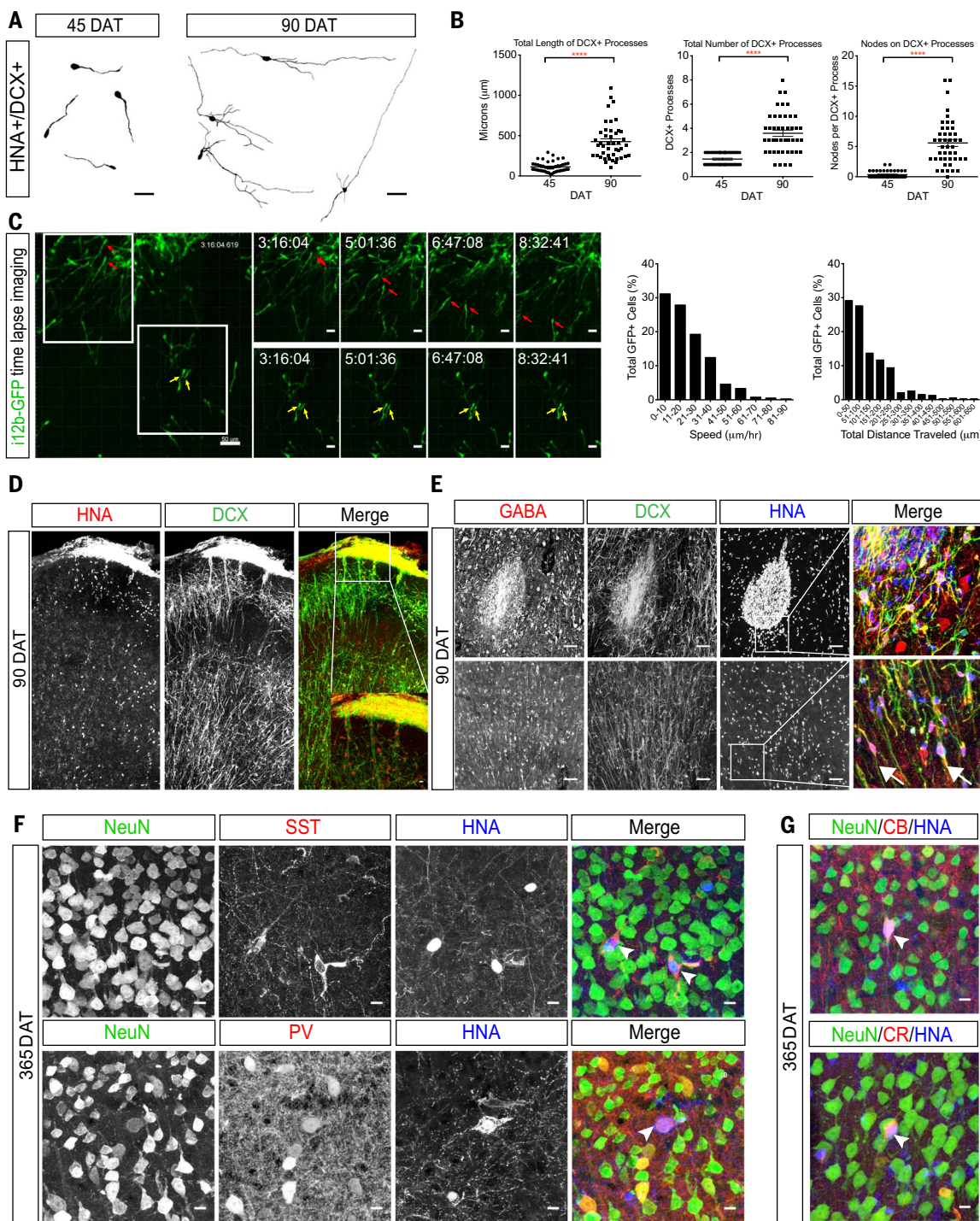


Fig. 5. Transplanted hMGE cells display migratory and functional interneuronal features. (A) Neurolucida tracings of DCX⁺ transplanted hMGE at 45 and 90 DAT (four cells shown per time point). (B) Quantification of the length (left) and total number (center) of DCX-positive processes at 45 and 90 DAT. Right graph shows quantification of the number of DCX⁺ branching nodes per transplanted cell analyzed at 45 or 90 DAT. For all graphs, $n = 22$ cells per animal for both 45 and 90 DAT; ****P < 0.0001. (C) Left: Sequential images of time-lapse confocal microscopy showing two example sets (red and yellow arrows) of GFP⁺ transplanted hMGE cells at 21 DAT. Right: Proportion of GFP-positive transplanted hMGE cells (total 395 cells) analyzed for speed (left) and total distance traveled (right).

(D) Confocal image of transplanted mouse cortex at 90 DAT showing dispersal of HNA⁺DCX⁺ cells. Inset shows boxed area at higher magnification. (E) Top: Injection site at 90 DAT contains cells that coexpress DCX, GABA, and HNA. Bottom: Transplanted hMGE cells away from the injection site also coexpress DCX and GABA (arrows). (F) Examples of transplanted hMGE cells at 365 DAT that express NeuN (green) and HNA (blue) either with SST (red, arrowheads in top panel) or PV (red, arrowhead in bottom panel). (G) Examples of transplanted hMGE cells at 365 DAT that express NeuN, calbindin (CB⁺, arrowhead in top), and calretinin (CR⁺, arrowhead in bottom). Scale bars, 50 μ m [(A), (C) (leftmost panel), (E)], 25 μ m [(C) (upper and lower rows)], 10 μ m [(D) (inset), (F), (G)].

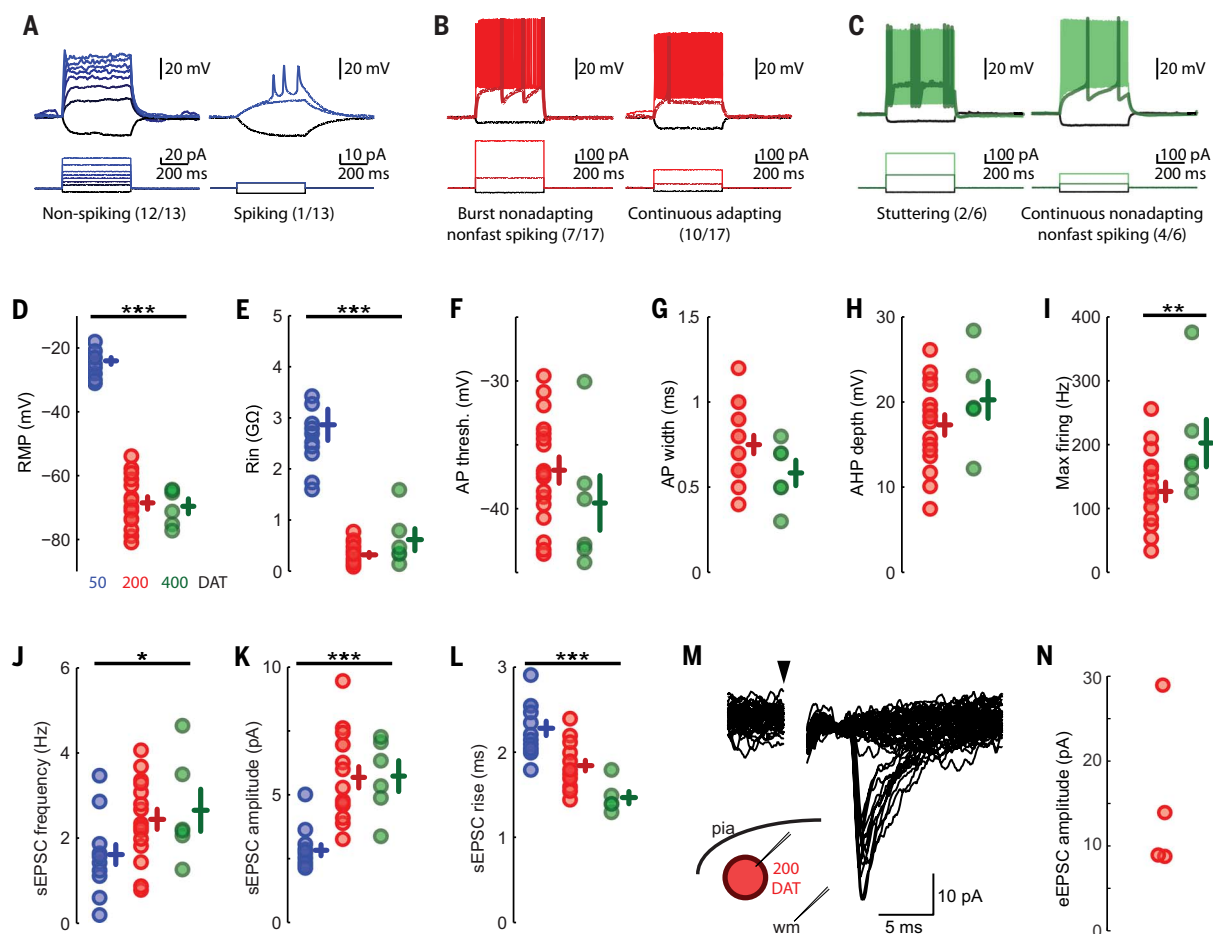


Fig. 6. Physiological parameters of hMGE cells after transplantation.

(A) hMGE cells at 50 DAT demonstrate immature action potentials with either minimal regenerative current (left) or a few short/broad action potentials (right). (B) hMGE cells at 200 DAT have regenerative action potentials (17/17 tested) that occur in one of two distinct temporal patterns, either burst nonadapting nonfast spiking (left) or continuous adapting (right). (C) hMGE cells at 400 DAT have action potentials in either a stuttering pattern (left) characteristic of fast-spiking interneurons or a continuous nonadapting phenotype (right). (D and E) Passive physiological properties changed over maturation with a significant hyperpolarization of resting membrane potential [(D), $P < 10^{-18}$ by one-way analysis of variance (ANOVA)] and a significant decrease in input resistance [(E), $P < 10^{-10}$ by one-way ANOVA]. (F to I) Active membrane

properties were not assessed in 50 DAT transplant-derived cells because they almost uniformly did not fire action potentials. There were no significant changes to the action potential threshold (F) or width (G), the action potential after hyperpolarization (AHP) depth (H), or the maximal firing rate [(I), by two-sample Kolmogorov-Smirnov test]. (J) All cells recorded had clearly identifiable EPSCs at 50 DAT, but sEPSC frequency increased significantly at 200 and 400 DAT ($P = 0.038$ by one-way ANOVA). (K and L) sEPSC amplitude also increased upon maturation ($P < 10^{-5}$ by one-way ANOVA) (K), whereas rise time decreased (L) ($P < 10^{-6}$ by one-way ANOVA). (M and N) EPSCs evoked by deep white matter stimulation $>500 \mu\text{m}$ from the recorded soma (M) demonstrate small eEPSCs (20 sequential traces at minimal stimulation amplitude) in all cells in which extracellular stimulation was attempted (N). * $P < 0.05$, ** $P < 0.01$, *** $P < 0.001$.

F and G). Patch-clamp recording in slices prepared at 50 DAT showed that the majority (12/13) of GFP⁺ hMGE-derived cells had immature action potential with minimal regenerative currents. Only one recorded cell at 50 DAT showed spiking in response to current injections (Fig. 6A, right). At 200 DAT, all hMGE-derived neurons (17 GFP⁺ cells) had mature action potentials and could be classified by their firing patterns into continuous adapting or burst nonadapting (Fig. 6B). By 400 DAT, recorded GFP⁺ cells exhibited action potentials with stuttering patterns characteristic of fast-spiking GABAergic interneurons (2/6 GFP⁺ cells) or a continuous nonadapting phenotype (Fig. 6C). Synaptic input in the

hMGE-derived cells was detected as early as 50 DAT. By 200 DAT, white matter stimulation elicited evoked excitatory postsynaptic currents (eEPSCs) in all recorded cells (Fig. 6, M and N) indicating that hMGE-derived neurons were integrated into the host mouse brain. These results demonstrate that a subpopulation of hMGE-derived cells transplanted into the mouse brain migrates widely and matures into functional interneuron subtypes that receive synaptic input.

Discussion

Our results reveal that the hMGE is organized into nests of DCX⁺ cells (DENs) containing proliferative neuroblasts (Fig. 7). DENs are

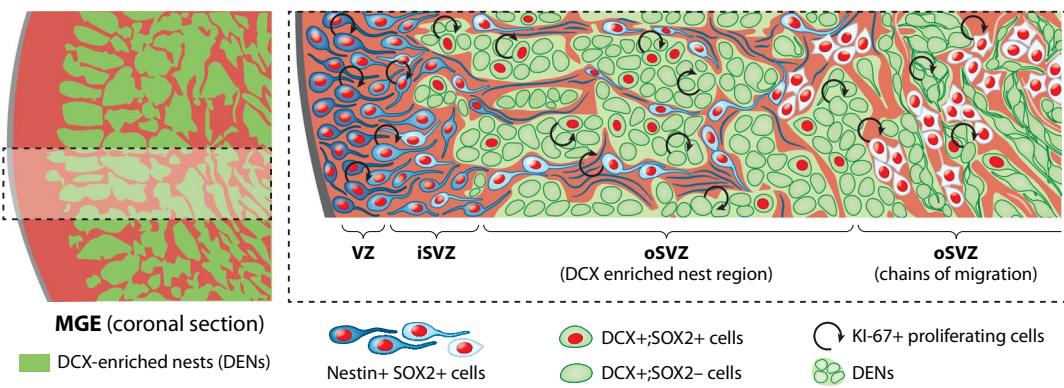
surrounded by nestin⁺ progenitors, an arrangement not observed in the rodent MGE (5, 31, 32) or in other germinal zones of the human forebrain, including the LGE or the pallium (10). DENs are also not apparent in the human CGE (10), another major source of cortical interneurons (11, 33, 34). Furthermore, transplantation of hMGE cells into the rodent brain formed DENs containing proliferative DCX⁺ cells and gave rise to GABAergic interneuron subtypes. These results suggest that DENs are formed by cell-autonomous mechanisms and give rise to highly migratory cells that differentiate into GABAergic interneurons.

Do DCX⁺/SOX2⁺ cells represent an intermediate or transient amplifying progenitor state?

Fig. 7. The developing hMGE contains multiple layers of proliferating nestin⁺ progenitors and DCX⁺ neuroblasts.

Left: Schematic overview of hMGE showing organization of progenitor regions (red) surrounding DCX⁺ cells (green regions). Right: Higher magnification of the boxed area at left. DCX⁺ cells (green) are organized into DENs surrounded by nestin⁺/SOX2⁺ progenitors (illustrated in different shades of blue to white).

Cell proliferation was observed among DCX⁺ cells in DENs until the end of gestation (see text). Nestin⁺/SOX2⁺ progenitors are also proliferative and are found within the VZ, the inner SVZ (iSVZ), and around DENs in the outer SVZ (oSVZ). Nestin⁺ progenitors and fibers surround DENs and are organized into tight bundles, previously identified as type I clusters (10) (light blue cells) in the initial segment of the oSVZ. In the outer part of the oSVZ, DENs transition to chains of migrating cells, and nestin⁺ progenitor cells are arranged as type II clusters (10). [Illustration by Noel Sirivansanti]



SOX2 is a transcription factor present in stem cells and is necessary for their progression to neural fates. Yet SOX2 also functions to maintain proliferation (35–37). Therefore, the presence of SOX2 could maintain a proliferative state in a subpopulation of DCX⁺ cells that are already committed to become inhibitory interneurons expressing GABA (DLX2⁺). It remains unknown how SOX2 expression is maintained in a subset of DCX⁺ cells within the hMGE. Nor is it known whether these cells divide symmetrically to amplify their population, or divide asymmetrically to retain a population of less differentiated progenitors. Proliferation in the hMGE was also highlighted by the expression of E2F1 among DCX⁺ cells within the DENs (fig. S3). The E2F family is involved in regulating the cell cycle (38–40) and could also function in maintaining the proliferative properties of DCX⁺ cells in DENs.

Work in the rodent brain has shown that the MGE is also an important source of oligodendrocytes (41, 42). We found large numbers of OLIG2⁺ cells in the hMGE, but these cells were found outside the DENs from 15 to 39 GW (fig. S3, E and F). We also observed a pronounced expansion of oligodendrocyte progenitors from hMGE transplants at 210 and 365 DAT (fig. S9C). Oligodendrocyte progenitor cells continue to divide after they leave the MGE (43); this suggests that unlike interneuron precursor proliferation, which seems to be closely linked to DENs, oligodendrocyte amplification can occur outside the MGE.

How are DENs formed? Electron microscopy revealed frequent adhesion contacts between cells within DENs, providing multiple sites to anchor DEN cells together. Our data also showed that cells within DENs express PCDH19, whereas nestin⁺ progenitors surrounding DENs express PCDH10, suggesting a role for differential cell adhesion in the

formation and maintenance of DENs. Mutations in *PCDH19* have been causally linked to epilepsy in females with mental retardation (EFMR), whereas variants of human *PCDH10* have been associated with autism (44).

The diversity of interneurons has evolved across species, including the presence of unique interneuron subtypes in humans and a reallocation of interneuron subtypes in primate brains (45, 46). Previous work has suggested that distinct ventrodorsal levels of the mouse MGE generate different subtypes of cortical interneurons (47). We found that the size of DENs within the MGE, and the proportion of the MGE occupied by DENs, varies depending on the dorsoventral level (Fig. 1). DENs in different regions of the hMGE may represent expansion of different subtypes of interneurons. The presence of a distinctive neurogenic niche with spatially discrete nests of proliferating DCX⁺ cells could contribute to differences in interneuron populations across organisms. Discovering the mechanisms underlying cortical interneuron production in the hMGE will also provide insight into the cell types and developmental periods that are vulnerable to genetic or environmental insults.

Methods summary

We studied human MGE samples from 14 to 39 gestational weeks. Tissues were collected with previous patient consent according to institutional ethical regulations of the University of California San Francisco Committee on Human Research. Histological sections were generated from human MGE tissues for immunohistochemistry and *in situ* hybridization to identify young neurons, progenitor cells, and molecular markers for proliferation, intermediate progenitor states, and transcription factors associated with the ganglionic eminences. To determine the MGE volume and changes through gestational stages, we performed volumetric measurements of hMGE

in MRI and combined them with immunohistochemical and immunofluorescence staining. We used transmission electron microscopy to perform an ultrastructural analysis of the cellular composition of the hMGE and identification of DEN cells at 14, 17, and 23 GW. To identify DCX⁺ cells and nestin radial glial fibers under TEM, we performed immunogold staining against these markers. To identify the MGE pattern of gene expression compared to LGE, we performed transcriptomic analysis on publicly available gene expression data of the human ganglionic eminences from the Allen Institute. Analyses were on laser-microdissected CNS bulk tissue from four prenatal human brains at 17 to 23 GW. (23). Unsupervised gene coexpression module detection and identification of region-specific modules revealed genes associated with the MGE that were validated in the human tissue sections. To determine the proliferative capacity of the human MGE ex vivo, we generated organotypic slice cultures from the human MGE that were infected with CMV-GFP adenovirus and imaged for 3 days using time-lapse confocal imaging. We performed xenograft experiments transplanting human MGE cells into immunocompromised neonatal mice and analyzed brains at 45, 90, 210, and 400 days after transplantation. Transplanted brains were used for histological analysis and to generate live tissue sections for migration assays and electrophysiology experiments.

REFERENCES AND NOTES

- R. Canitano, M. Pallagrosi, Autism Spectrum Disorders and Schizophrenia Spectrum Disorders: Excitation/Inhibition Imbalance and Developmental Trajectories. *Front. Psychiatry* **8**, 69 (2017). doi: 10.3389/fpsyg.2017.00069; pmid: 28507523
- B. Chattopadhyaya, G. D. Cristo, GABAergic circuit dysfunctions in neurodevelopmental disorders. *Front. Psychiatry* **3**, 51 (2012). doi: 10.3389/fpsyg.2012.00051; pmid: 22666213
- O. Marin, Interneuron dysfunction in psychiatric disorders. *Nat. Rev. Neurosci.* **13**, 107–120 (2012). doi: 10.1038/nrn3155; pmid: 22251963

4. C. P. Wonders, S. A. Anderson, The origin and specification of cortical interneurons. *Nat. Rev. Neurosci.* **7**, 687–696 (2006). doi: [10.1038/nrn1954](https://doi.org/10.1038/nrn1954); pmid: [16883309](https://pubmed.ncbi.nlm.nih.gov/16883309/)
5. S. A. Anderson, O. Marín, C. Horn, K. Jennings, J. L. Rubenstein, Distinct cortical migrations from the medial and lateral ganglionic eminences. *Development* **128**, 353–363 (2001). doi: [10.1242/dev.128.3.353](https://doi.org/10.1242/dev.128.3.353); pmid: [1152634](https://pubmed.ncbi.nlm.nih.gov/1152634/)
6. O. Marín, Cellular and molecular mechanisms controlling the migration of neocortical interneurons. *Eur. J. Neurosci.* **38**, 2019–2029 (2013). doi: [10.1111/ejn.12225](https://doi.org/10.1111/ejn.12225); pmid: [23651101](https://pubmed.ncbi.nlm.nih.gov/23651101/)
7. H. Wichterle, J. M. García-Verdugo, D. G. Herrera, A. Alvarez-Buylla, Young neurons from medial ganglionic eminence disperse in adult and embryonic brain. *Nat. Neurosci.* **2**, 461–466 (1999). doi: [10.1038/8131](https://doi.org/10.1038/8131); pmid: [10321251](https://pubmed.ncbi.nlm.nih.gov/10321251/)
8. V. S. Sohal, F. Zhang, O. Yizhar, K. Deisseroth, Parvalbumin neurons and gamma rhythms enhance cortical circuit performance. *Nature* **459**, 698–702 (2009). doi: [10.1038/nature07991](https://doi.org/10.1038/nature07991); pmid: [19396159](https://pubmed.ncbi.nlm.nih.gov/19396159/)
9. B. R. Ferguson, W.-J. Gao, Thalamic Control of Cognition and Social Behavior Via Regulation of γ -Aminobutyric Acidergic Signaling and Excitation/Inhibition Balance in the Medial Prefrontal Cortex. *Biol. Psychiatry* **83**, 657–669 (2018). doi: [10.1016/j.biopsych.2017.11.033](https://doi.org/10.1016/j.biopsych.2017.11.033); pmid: [29373121](https://pubmed.ncbi.nlm.nih.gov/29373121/)
10. D. V. Hansen et al., Non-epithelial stem cells and cortical interneuron production in the human ganglionic eminences. *Nat. Neurosci.* **16**, 1576–1587 (2013). doi: [10.1038/nn.3541](https://doi.org/10.1038/nn.3541); pmid: [24097039](https://pubmed.ncbi.nlm.nih.gov/24097039/)
11. T. Ma et al., Subcortical origins of human and monkey neocortical interneurons. *Nat. Neurosci.* **16**, 1588–1597 (2013). doi: [10.1038/nn.3536](https://doi.org/10.1038/nn.3536); pmid: [24097041](https://pubmed.ncbi.nlm.nih.gov/24097041/)
12. C. Stuhdholme, Mapping the developing human brain in utero using quantitative MR imaging techniques. *Semin. Perinatol.* **39**, 105–112 (2015). doi: [10.1053/j.semperi.2015.01.003](https://doi.org/10.1053/j.semperi.2015.01.003); pmid: [25813665](https://pubmed.ncbi.nlm.nih.gov/25813665/)
13. J. A. Scott et al., Growth trajectories of the human fetal brain tissues estimated from 3D reconstructed in utero MRI. *Int. J. Dev. Neurosci.* **29**, 529–536 (2011). doi: [10.1016/j.ijdevneu.2011.04.001](https://doi.org/10.1016/j.ijdevneu.2011.04.001); pmid: [21530634](https://pubmed.ncbi.nlm.nih.gov/21530634/)
14. D. Vogt et al., Lhx6 directly regulates Arx and CXCR7 to determine cortical interneuron fate and laminar position. *Neuron* **82**, 350–364 (2014). doi: [10.1016/j.neuron.2014.02.030](https://doi.org/10.1016/j.neuron.2014.02.030); pmid: [24742460](https://pubmed.ncbi.nlm.nih.gov/24742460/)
15. P. Liodis et al., Lhx6 activity is required for the normal migration and specification of cortical interneuron subtypes. *J. Neurosci.* **27**, 3078–3089 (2007). doi: [10.1523/JNEUROSCI.3055-06.2007](https://doi.org/10.1523/JNEUROSCI.3055-06.2007); pmid: [17376969](https://pubmed.ncbi.nlm.nih.gov/17376969/)
16. J. Stenman, H. Toresson, K. Campbell, Identification of two distinct progenitor populations in the lateral ganglionic eminence: Implications for striatal and olfactory bulb neurogenesis. *J. Neurosci.* **23**, 167–174 (2003). doi: [10.1523/JNEUROSCI.23-01-00167.2003](https://doi.org/10.1523/JNEUROSCI.23-01-00167.2003); pmid: [12514213](https://pubmed.ncbi.nlm.nih.gov/12514213/)
17. M. A. Petryniak, G. B. Potter, D. H. Rowitch, J. L. R. Rubenstein, Dlx1 and Dlx2 control neuronal versus oligodendroglial cell fate acquisition in the developing forebrain. *Neuron* **55**, 417–433 (2007). doi: [10.1016/j.neuron.2007.06.036](https://doi.org/10.1016/j.neuron.2007.06.036); pmid: [17678855](https://pubmed.ncbi.nlm.nih.gov/17678855/)
18. J. E. Long, I. Cobos, G. B. Potter, J. L. R. Rubenstein, Dlx1&2 and Mash1 transcription factors control MGE and CGE patterning and differentiation through parallel and overlapping pathways. *Cereb. Cortex* **19** (suppl. 1), i96–i106 (2009). doi: [10.1093/cercor/bhp045](https://doi.org/10.1093/cercor/bhp045); pmid: [19386638](https://pubmed.ncbi.nlm.nih.gov/19386638/)
19. C. Lois, J. M. García-Verdugo, A. Alvarez-Buylla, Chain migration of neuronal precursors. *Science* **271**, 978–981 (1996). doi: [10.1126/science.271.5251.978](https://doi.org/10.1126/science.271.5251.978); pmid: [8584933](https://pubmed.ncbi.nlm.nih.gov/8584933/)
20. M. F. Paredes et al., Extensive migration of young neurons into the infant human frontal lobe. *Science* **354**, aaf0703 (2016). doi: [10.1126/science.aaf0703](https://doi.org/10.1126/science.aaf0703); pmid: [27846470](https://pubmed.ncbi.nlm.nih.gov/27846470/)
21. H. Guerrero-Cázares et al., Cytoarchitecture of the lateral ganglionic eminence and rostral extension of the lateral ventricle in the human fetal brain. *J. Comp. Neurol.* **519**, 1165–1180 (2011). doi: [10.1002/cne.22566](https://doi.org/10.1002/cne.22566); pmid: [21344407](https://pubmed.ncbi.nlm.nih.gov/21344407/)
22. A. Cebrán-Silla et al., Unique Organization of the Nuclear Envelope in the Post-natal Quiescent Neural Stem Cells. *Stem Cell Rep.* **9**, 203–216 (2017). doi: [10.1016/j.stemcr.2017.05.024](https://doi.org/10.1016/j.stemcr.2017.05.024); pmid: [28648897](https://pubmed.ncbi.nlm.nih.gov/28648897/)
23. J. A. Miller et al., Transcriptional landscape of the prenatal human brain. *Nature* **508**, 199–206 (2014). doi: [10.1038/nature13185](https://doi.org/10.1038/nature13185); pmid: [24695229](https://pubmed.ncbi.nlm.nih.gov/24695229/)
24. K. W. Kelley, H. Nakao-Inoue, A. V. Molofsky, M. C. Oldham, Variation among intact tissue samples reveals the core transcriptional features of human CNS cell classes. *Nat. Neurosci.* **21**, 1171–1184 (2018). doi: [10.1038/s41593-018-0216-z](https://doi.org/10.1038/s41593-018-0216-z); pmid: [30154505](https://pubmed.ncbi.nlm.nih.gov/30154505/)
25. M. Götz, S. Sirko, J. Beckers, M. Irmler, Reactive astrocytes as neural stem or progenitor cells: In vivo lineage, In vitro potential, and Genome-wide expression analysis. *Glia* **63**, 1452–1468 (2015). doi: [10.1002/glia.22850](https://doi.org/10.1002/glia.22850); pmid: [25965557](https://pubmed.ncbi.nlm.nih.gov/25965557/)
26. M. Komitova, P. S. Eriksson, Sox-2 is expressed by neural progenitors and astroglia in the adult rat brain. *Neurosci. Lett.* **369**, 24–27 (2004). doi: [10.1016/j.neulet.2004.07.035](https://doi.org/10.1016/j.neulet.2004.07.035); pmid: [15380301](https://pubmed.ncbi.nlm.nih.gov/15380301/)
27. D. V. Hansen, J. H. Lui, P. R. L. Parker, A. R. Kriegstein, Neurogenic radial glia in the outer subventricular zone of human neocortex. *Nature* **464**, 554–561 (2010). doi: [10.1038/nature08845](https://doi.org/10.1038/nature08845); pmid: [20154730](https://pubmed.ncbi.nlm.nih.gov/20154730/)
28. D. G. Southwell et al., Interneurons from embryonic development to cell-based therapy. *Science* **344**, 1240622 (2014). doi: [10.1126/science.1240622](https://doi.org/10.1126/science.1240622); pmid: [24723614](https://pubmed.ncbi.nlm.nih.gov/24723614/)
29. S. Nóbrega-Pereira et al., Postmitotic Nkx2-1 controls the migration of telencephalic interneurons by direct repression of guidance receptors. *Neuron* **59**, 733–745 (2008). doi: [10.1016/j.neuron.2008.07.024](https://doi.org/10.1016/j.neuron.2008.07.024); pmid: [18786357](https://pubmed.ncbi.nlm.nih.gov/18786357/)
30. O. Marín et al., Directional guidance of interneuron migration to the cerebral cortex relies on subcortical Slit1/2-independent repulsion and cortical attraction. *Development* **130**, 1889–1901 (2003). doi: [10.1242/dev.00417](https://doi.org/10.1242/dev.00417); pmid: [12642493](https://pubmed.ncbi.nlm.nih.gov/12642493/)
31. J. S. Hu, D. Vogt, M. Sandberg, J. L. Rubenstein, Cortical interneuron development: A tale of time and space. *Development* **144**, 3867–3878 (2017). doi: [10.1242/dev.132852](https://doi.org/10.1242/dev.132852); pmid: [29089360](https://pubmed.ncbi.nlm.nih.gov/29089360/)
32. G. Paxinos, G. Halliday, C. Watson, M. S. Kassem, *Atlas of the Developing Mouse Brain* (Academic Press, 2020).
33. S. Nery, G. Fishell, J. G. Corbin, The caudal ganglionic eminence is a source of distinct cortical and subcortical cell populations. *Nat. Neurosci.* **5**, 1279–1287 (2002). doi: [10.1038/nn971](https://doi.org/10.1038/nn971); pmid: [12411960](https://pubmed.ncbi.nlm.nih.gov/12411960/)
34. L. Lim, D. Mi, A. Llorca, O. Marín, Development and Functional Diversification of Cortical Interneurons. *Neuron* **100**, 294–313 (2018). doi: [10.1016/j.neuron.2018.10.009](https://doi.org/10.1016/j.neuron.2018.10.009); pmid: [30359598](https://pubmed.ncbi.nlm.nih.gov/30359598/)
35. V. Graham, J. Khudyakov, P. Ellis, L. Pevny, SOX2 functions to maintain neural progenitor identity. *Neuron* **39**, 749–765 (2003). doi: [10.1016/S0896-6273\(03\)00497-5](https://doi.org/10.1016/S0896-6273(03)00497-5); pmid: [12948443](https://pubmed.ncbi.nlm.nih.gov/12948443/)
36. S. Gómez-López et al., Sox2 and Pax6 maintain the proliferative and developmental potential of gliogenic neural stem cells In vitro. *Glia* **59**, 1588–1599 (2011). doi: [10.1002/glia.21201](https://doi.org/10.1002/glia.21201); pmid: [21766338](https://pubmed.ncbi.nlm.nih.gov/21766338/)
37. D. W. Hagey et al., SOX2 regulates common and specific stem cell features in the CNS and endoderm derived organs. *PLOS Genet.* **14**, e1007224 (2018). doi: [10.1371/journal.pgen.1007224](https://doi.org/10.1371/journal.pgen.1007224); pmid: [29432416](https://pubmed.ncbi.nlm.nih.gov/29432416/)
38. L. Magri et al., E2F1 coregulates cell cycle genes and chromatin components during the transition of oligodendrocyte progenitors from proliferation to differentiation. *J. Neurosci.* **34**, 1481–1493 (2014). doi: [10.1523/JNEUROSCI.2840-13.2014](https://doi.org/10.1523/JNEUROSCI.2840-13.2014); pmid: [24453336](https://pubmed.ncbi.nlm.nih.gov/24453336/)
39. K. Ohtani, J. DeGregori, J. R. Nevins, Regulation of the cyclin E gene by transcription factor E2F1. *Proc. Natl. Acad. Sci. U.S.A.* **92**, 12146–12150 (1995). doi: [10.1073/pnas.92.26.12146](https://doi.org/10.1073/pnas.92.26.12146); pmid: [8618861](https://pubmed.ncbi.nlm.nih.gov/8618861/)
40. P.-D. Denechaud, L. Fajas, A. Giralt, E2F1, a Novel Regulator of Metabolism. *Front. Endocrinol.* **8**, 311 (2017). doi: [10.3389/fendo.2017.00311](https://doi.org/10.3389/fendo.2017.00311); pmid: [29176962](https://pubmed.ncbi.nlm.nih.gov/29176962/)
41. N. Kessaris et al., Competing waves of oligodendrocytes in the forebrain and postnatal elimination of an embryonic lineage. *Nat. Neurosci.* **9**, 173–179 (2006). doi: [10.1038/nn1620](https://doi.org/10.1038/nn1620); pmid: [16388308](https://pubmed.ncbi.nlm.nih.gov/16388308/)
42. S. A. Goldman, N. J. Kuypers, How to make an oligodendrocyte. *Development* **142**, 3983–3995 (2015). doi: [10.1242/dev.126409](https://doi.org/10.1242/dev.126409); pmid: [26628089](https://pubmed.ncbi.nlm.nih.gov/26628089/)
43. W. Huang et al., Origins and Proliferative States of Human Oligodendrocyte Precursor Cells. *Cell* **182**, 594–608.e11 (2020). doi: [10.1016/j.cell.2020.06.027](https://doi.org/10.1016/j.cell.2020.06.027); pmid: [32679030](https://pubmed.ncbi.nlm.nih.gov/32679030/)
44. E. Morrow et al., Identifying autism loci and genes by tracing recent shared ancestry. *Science* **321**, 218–223 (2008). doi: [10.1126/science.1157657](https://doi.org/10.1126/science.1157657); pmid: [18621663](https://pubmed.ncbi.nlm.nih.gov/18621663/)
45. F. M. Krienen et al., Innovations present in the primate interneuron repertoire. *Nature* **586**, 262–269 (2020). doi: [10.1038/s41586-020-2781-z](https://doi.org/10.1038/s41586-020-2781-z); pmid: [32999462](https://pubmed.ncbi.nlm.nih.gov/32999462/)
46. E. Boldog et al., Transcriptomic and morphophysiological evidence for a specialized human cortical GABAergic cell type. *Nat. Neurosci.* **21**, 1185–1195 (2018). doi: [10.1038/s41593-018-0205-2](https://doi.org/10.1038/s41593-018-0205-2); pmid: [30150662](https://pubmed.ncbi.nlm.nih.gov/30150662/)
47. N. Flames et al., Delineation of multiple subpallial progenitor domains by the combinatorial expression of transcriptional codes. *J. Neurosci.* **27**, 9682–9695 (2007). doi: [10.1523/JNEUROSCI.2750-07.2007](https://doi.org/10.1523/JNEUROSCI.2750-07.2007); pmid: [17804629](https://pubmed.ncbi.nlm.nih.gov/17804629/)

ACKNOWLEDGMENTS

We thank and honor the families who generously donated the tissue samples used in this study. A. Paredes for editing comments, and E. Marsan for data analysis discussion. **Funding:** R25 NS070680 (P.L. and J.A.C.); R01 MH113896 (M.C.O.); R01 EB017133, R01 NS055064, and NSF CRCNS 2011088 (C.S.); P01 NS083513 (A.A.-B., M.F.P., A.R.K., and E.J.H.); K08 NS091537 (M.F.P.); R01 NS028478 (A.A.-B.); AHA Predoctoral Fellowship 19PRE3480616 (J.Chen); Roberta and Oscar Gregory Endowment in Stroke and Brain Research (M.F.P.); Valencian Council for Innovation, Universities, Sciences and Digital Society (PROMETEO/2019/075) and Red de Terapia Celular (TerCel-RD16/0011/0026) (J.M.G.-V.); Spanish Generalitat Valenciana and European Social Fund Postdoctoral Fellowship (APOSTD2018/A113) (A.C.-S.); and CIRM Bridges (EDUC2-126-93) (C.M.) **Author contributions:** M.F.P., A.A.-B., and E.J.H. designed the study with assistance from J.A.C., C.M., and Q.F.-R.; C.M., Q.F.-R., A.D.D., J. Chen, J. Chu, E.G., J.A.C., V.T., and J.S. performed the histological work with the postmortem samples and analyzed the data; J.S. and C.S. performed the analysis on the prenatal MRI datasets; A.C.-S. and S.G.G. performed the ultrastructural analysis under the supervision of J.M.G.-V.; R.D. and T.J.N. performed live imaging analysis; P.L. and A.H. performed and led the electrophysiological studies; G.K. and M.C.O. performed the bioinformatics analysis of hMGE and hLGE RNA datasets; A.R.K., J.F.L., and M.V. contributed tissue resources and data interpretation; and M.F.P., C.M., Q.F.-R., A.C.-S., A.A.-B., and E.J.H. wrote the manuscript with feedback from all authors. **Competing interests:** P.L. is currently an employee of Vertex Pharmaceuticals and owns shares in the company. A.A.-B. is co-founder and on the scientific advisory board of Neurona Therapeutics. **Data and materials availability:** All data are available in the main text or the supplementary materials.

SUPPLEMENTARY MATERIALSscience.org/doi/10.1126/science.abk2346

Materials and Methods

Figs. S1 to S12

Tables S1 to S3

References (48–57)

Movies S1 to S3

10 July 2021; accepted 1 December 2021

10.1126/science.abk2346